Supporting Information

Mesostructuring layered materials: self-supported mesoporous layered double hydroxide nanotubes

*Alysson F. Morais, Dimy Nanclares, Ivan G.N. Silva, Alfredo Duarte, Fernando A. Garcia, Eric Breynaert and Danilo Mustafa**

S1. Materials and Methods

The metal precursors $Zn(NO_3)_2 \cdot 6H_2O$ (98 mol%, Vetec) and $Al(NO_3)_3 \cdot 9H_2O$ (98 mol%, LabSynth), H_3BTC (97 mol%, Sigma-Aldrich, powder form) and NaOH (97 mol%, Vetec, lentils) were used without further purification. $Eu(NO_3)_3 \cdot 6H_2O$ was prepared by dissolution of Eu_2O_3 (CSTARM, 99,99 mol%) in concentrated nitric acid and subsequent crystallization of $Eu(NO_3)_3.6H_2O$. The triblock copolymer Pluronic® P-123 was procured from Sigma Aldrich (São Paulo, Brazil).

S1.1. Synthesis

Mesoporous LDH with nominal composition $[Zn_2Al_{1-X}Eu_X(OH)_6]^{\cdot}(BTC^{3-})_{0.33}.pH_2O$, dubbed ZnAl-BTC-P123 for X = 0 and ZnAlEuX-BTC-P123 for X = 0.5, 1, 3, 5, 10 and 15%, were synthesized by coprecipitation of Zn^{2+}, Al^{3+} and Eu^{3+} in alkaline solution containing BTC and Pluronic® P-123 worm-like micelles. To prepare the micelles, 200 mL of a solution containing 0.15 wt% P-123 and 11.5 x 10^{-3} $mol.L^{-1}$ BTC and whose pH was adjusted to pH 8 with addition of sodium hydroxide were heated to 60°C to complete dissolution of the components and subsequently cooled to room temperature. Another heat cycle to 60 °C was done to optimize the micellization. To prepare the LDHs, 10 mL of a solution containing the metal precursors $Zn(NO_3)_2 \cdot 6H_2O$, $Al(NO_3)_3 \cdot 9H_2O$ and $Eu(NO_3)_3 \cdot 6H_2O$ in the ratio 2:1-X:X and total metal concentration of 1 $mol.L^{-1}$ (see **Table S1**) were dosed at a rate of 10 $mL.h^{-1}$ into the solution containing the BTC and the micelles. The pH of the synthesis solution was stated at pH 8 by a Metrohm 848 Titrino plus automatic titrator. Finished the metal solution, the resulting suspension was aged statically in a closed vessel at 60 °C for two days, followed by

centrifugation and rinsing with distilled water. To remove P-123 from the samples, the resulting slurry was re-suspended twice in methanol and sonicated for 15 min. The material was dried in oven at 60°C for three days. Flake-like LDHs with nominal composition $[Zn_2Al(OH)_6]\cdot(NO_3^-).yH_2O$, $[Zn_2Al_{0.95}Eu_{0.05}(OH)_6]\cdot(NO_3^-).zH_2O$, and $[Zn_2Al_{0.95}Eu_{0.05}(OH)_6]\cdot(BTC^{3-})_{0.33}.wH_2O$, dubbed, respectively, ZnAl-NO_3, ZnAlEu5%-NO_3 and ZnAlEu5%-BTC, were synthetized with the same synthetic procedure, but without addition of P-123 and without heating. For ZnAl-NO_3 and ZnAlEu5%-NO_3 no BTC was added (see **Table S1**).

Table S1. Synthetic conditions: concentration of Zn^{3+}, Al^{3+} and Eu^{3+} for each of the samples

Sample	$[Zn^{2+}]$ $(mol.L^{-1})$	$[Al^{3+}]$ $(mol.L^{-1})$	$[Eu^{3+}]$ $(mol.L^{-1})$	BTC	P-123
ZnAl-NO_3	0.667	0.333	-	No	No
ZnAlEu5%-BTC	0.667	0.316	0.0166	Yes	No
ZnAlEu0%-BTC-P123	0.667	0.333	-	Yes	Yes
ZnAlEu0.5%-BTC-P123	0.667	0.331	0.00166	Yes	Yes
ZnAlEu1%-BTC-P123	0.667	0.330	0.00333	Yes	Yes
ZnAlEu3%-BTC-P123	0.667	0.323	0.00999	Yes	Yes
ZnAlEu5%-BTC-P123	0.667	0.316	0.0166	Yes	Yes
ZnAlEu10%-BTC-P123	0.667	0.300	0.0333	Yes	Yes
ZnAlEu15%-BTC-P123	0.667	0.283	0.0500	Yes	Yes

S1.2. Characterization

The Zinc, Aluminum, Europium, Carbon, Hydrogen and Nitrogen content in the samples were determined by elemental analysis. A Perkin Elmer (Massachusetts, EUA) 2400 series ii elemental analyzer was used for CHN analysis. For the metal content, Inductively Coupled Plasma Optical Emission Spectrometry (ICP-OES) was performed with a Spectro Arcos (SPECTRO Analytical Instruments GmbH, Germany) optical spectrometer with radial view. Thermogravimetric analysis (TG) was performed on a TGA Q500 (TA Instruments). The temperature was ramped up from room temperature to 800 °C at a rate of 5 °C min^{-1} using an air flow of 60 mL min^{-1}. Powder X-ray diffraction (PXRD) was performed using a D8 Discover (Bruker) diffractometer in Bragg-Brentano geometry (Cu

Kα radiation, λ = 1.5418 Å). Data was recorded for the 2θ range from 4° to 70° in steps of 0.05° using an integration time of 1 s. Photoluminescence spectra were measured with a SPEX® Fluorolog® 3 (Horiba) equipped with a 450 W Xenon lamp as excitation source. X-ray absorption near edge structure (XANES) and extended X-ray absorption fine structure (EXAFS) measurements were performed at the XAFS2 beamline of the Brazilian Synchrotron Light Laboratory (LNLS, Campinas, Brazil)[1]. A double-crystal Si(111) monochromator was used. The powder samples were pressed into pellets and the absorption spectra were measured in the fluorescence mode for the Eu L^{III}-edge (6.9769 keV). For the data analysis, an amplitude reduction factor $S_0^2 = 0.95 \pm 0.11$ has been obtained from the fitting of the Eu L^{III}-edge EXAFS data for the model compound Eu_2O_3 (cubic phase[2], coordination number = 6, see Ref. [3]). This value is in agreement with ab-initio calculations[4] using the FEFF8.4 code[5]. Chemical transferability has been assumed and this amplitude factor was used in the analysis of the LDH samples. The Demeter platform[6] has been used to model and fit the EXAFS data. Crystallographic information from layered Europium hydroxides[7], assumed to be crystal analogs for the local environment of Eu^{3+} in the LDHs, were used as input for the calculations implemented along with IFEFFIT.

S2. Chemical composition

The elemental analysis data is shown in **Table S2**. Thermogravimetric analysis was employed for the quantification of BTC from the mass loss event around 460 °C (**Figure S13**). The empirical formulae were derived assuming that, in line with the PXRD results, the general formula of the LDHs is valid for all samples with $Eu^{3+}/(Eu^{3+} + Al^{3+}) \leq 15\%$. Within the experimental uncertainties, the Zn^{2+}, Al^{3+} and + Eu^{3+} content in the samples agree with the nominal quantities added for the synthesis. The M^{II}/M^{III} metal fraction ranged from 2.0 to 2.34, close to the nominal fraction Zn/(Al+Eu) = 2. The BTC stoichiometry in the BTC-containing LDHs ranges from 0.38 to 0.58, indicating that a mixture of BTC^{2+} and BTC^{3+} are present in these samples.

Table S2. Experimental chemical composition of the samples.

Sample	Zn (mmol/g)	Al (mmol/g)	Eu (mmol/g)	C[B] (mmol/g)	H (mmol/g)	N (mmol/g)	BTC* (mmol/g)	Estimated formula[A]
ZnAl-NO_3	5.87(13)	2.73(1)	-	0.28(6)	24.5(2)	2.53(4)	-	$[Zn_{2.15}Al(OH)_{6.30}][(NO_3^-)_{0.93}(CO_3^{2-})_{0.10}].(1.5H_2O)$
ZnAlEu5%-NO_3	5.25(29)	2.49(19)	0.118(7)	0.36(5)	25.5(3)	2.39(5)	-	$[Zn_{2.01}Al_{0.955}Eu_{0.045}(OH)_{6.02}]\ [(NO_3^-)_{0.91}(CO_3^{2-})_{0.14}].(1.9H_2O)$
ZnAlEu5%-BTC	4.48(3)	2.13(2)	0.105(10)	11.2(2)	29.9(1)	0.06(1)	1.29	$[Zn_{2.00}Al_{0.953}Eu_{0.047}(OH)_{6.00}]\ [(NO_3^-)_{0.03}(BTC^{3-})_{0.57}].(2.8H_2O)$
ZnAl-BTC-P123	4.75(3)	2.33(1)	-	11.7(2)	32.3(3)	0,096(5)	0.69	$[Zn_{2.04}Al(OH)_{6.08}]\ [(NO_3^-)_{0.04}(BTC^{3-})_{0.30}].(nH_2O)$
ZnAlEu0.5%-BTC-P123	4.36(5)	2.16(3)	0.0137(1)	13.2(1)	33.0(3)	0.070(8)	0.95	$[Zn_{2.00}Al_{0.994}Eu_{0.006}(OH)_{6.00}]\ [(NO_3^-)_{0.03}(BTC^{3-})_{0.44}].(nH_2O)$
ZnAlEu1%-BTC-P123	4.58(21)	2.24(7)	0.0171(16)	12.7(1)	33.1(3)	0.09(3)	0.90	$[Zn_{2.03}Al_{0.992}Eu_{0.008}(OH)_{6.06}]\ [(NO_3^-)_{0.04}(BTC^{3-})_{0.40}].(nH_2O)$
ZnAlEu3%-BTC-P123	4.71(10)	2.11(6)	0.0730(13)	13.2(1)	32.7(1)	0.05(3)	0.95	$[Zn_{2.16}Al_{0.967}Eu_{0.033}(OH)_{6.32}]\ [(NO_3^-)_{0.02}(BTC^{3-})_{0.44}].(nH_2O)$
ZnAlEu5%-BTC-P123	4.51(3)	2.11(1)	0.117(1)	13.6(1)	33.1(1)	0.09(2)	0.85	$[Zn_{2.02}Al_{0.947}Eu_{0.052}(OH)_{6.04}]\ [(NO_3^-)_{0.04}(BTC^{3-})_{0.38}].(nH_2O)$
ZnAlEu10%-BTC-P123	4.68(3)	1.98(1)	0.243(1)	14.3(1)	29.2(1)	0.34(1)	1.29	$[Zn_{2.11}Al_{0.891}Eu_{0.109}(OH)_{6.22}]\ [(NO_3^-)_{0.15}(BTC^{3-})_{0.58}].(nH_2O)$
ZnAlEu15%-BTC-P123	3.64(29)	1.56(12)	0.199(27)	14.3(1)	34.5(1)	0.09(1)	0.85	$[Zn_{2.34}Al_{0.857}Eu_{0.143}(OH)_{6.68}]\ [(NO_3^-)_{0.05}(BTC^{3-})_{0.49}].(nH_2O)$

*** Calculated from TG. [A] For samples containing P123, the water content was not determined. [B] Both the Carbon content derived from CHN and TG agree for samples with no P123.**

S3. Structural characterization

Table S3. Crystallographic properties of the LDH samples.

Sample	Peak position $2\theta_{003}$ (°)	Peak width[a] $\delta(2\theta_{003})$ (°)	Basal spacing $d_{(003)}$ (Å)	Scherer crystallite size[b] - (003) direction - (nm)	Average number of stacked layers in a crystallite[c]
ZnAl-NO_3	9.88	0.92	8.95	9.2	10
ZnAlEu5%-NO_3	9.91	0.93	8.92	9.1	10
ZnAl-BTC	6.71	1.11	13.2	7.6	6
ZnAlEu5%-BTC	6.69	1.62	13.2	5.2	4
ZnAl-BTC-P123	6.91	1.38	12.8	6.1	5
ZnAlEu0.5%-BTC-P123	6.85	1.47	12.9	5.7	4
ZnAlEu1%-BTC-P123	6.66	1.37	13.3	6.1	5
ZnAlEu3%-BTC-P123	6.75	1.81	13.1	4.6	4
ZnAlEu5%-BTC-P123	6.80	1.93	13.0	4.3	3
ZnAlEu10%-BTC-P123	6.95	1.97	12.7	4.2	3
ZnAlEu15%-BTC-P123	7.00	1.73	12.6	4.8	4
ZnAlEu20%-BTC-P123	7.15	1.73	12.4	4.8	4

[a] Full width at half maximum. [b] Gaussian peak; Instrumental width: 0.14°. [c] Given by: (Crystallite size).(Basal spacing)$^{-1}$.

The interplanar spacing in hexagonal lattices is given by:

$$\frac{1}{d_{(hkl)}^{2}} = \frac{4}{3}\left(\frac{h^2 + hk + k^2}{a^2}\right) + \frac{l^2}{N^2 c_o^2},$$

where N, the stacking number, is the number of stacked layers within the unit cell.

Table S4. Indexing of the Bragg reflections for Zn_2Al-NO_3 with a rhombohedrally-centered hexagonal unit cell. Space group R3m; a = b = 3.064 Å and c = 3 c0 = 26.856 Å.

	Experimental		***Calculated***	
Reflection (hkl)	**Position** 2θ	**Interplanar spacing** $d_{(hkl)}$ **(Å)**	**Position** 2θ	**Interplanar spacing** $d_{(hkl)}$ **(Å)**
(003)	9.88	8.952	9.88	8.952
(006)	19.86	4.470	19.83	4.476
(009)	30.00	2.979	29.94	2.984
(101)	33.87	2.647	33.95	2.640
(012)	34.40	2.607	34.46	2.603
(104)	36.4(3)	2.468(19)	36.41	2.468
(015)	37.80	2.380	37.82	2.379
(018)	43.58	2.077	43.47	2.082
(1 0 10)	48.4(4)	1.881(15)	48.21	1.887
(0 1 11)	51.1(3)	1.787(11)	50.82	1.797
(0 1 13)	56.6(3)	1.626(8)	56.45	1.630
(110)	60.43	1.532	60.43	1.532
(113)	61.54	1.507	61.40	1.510

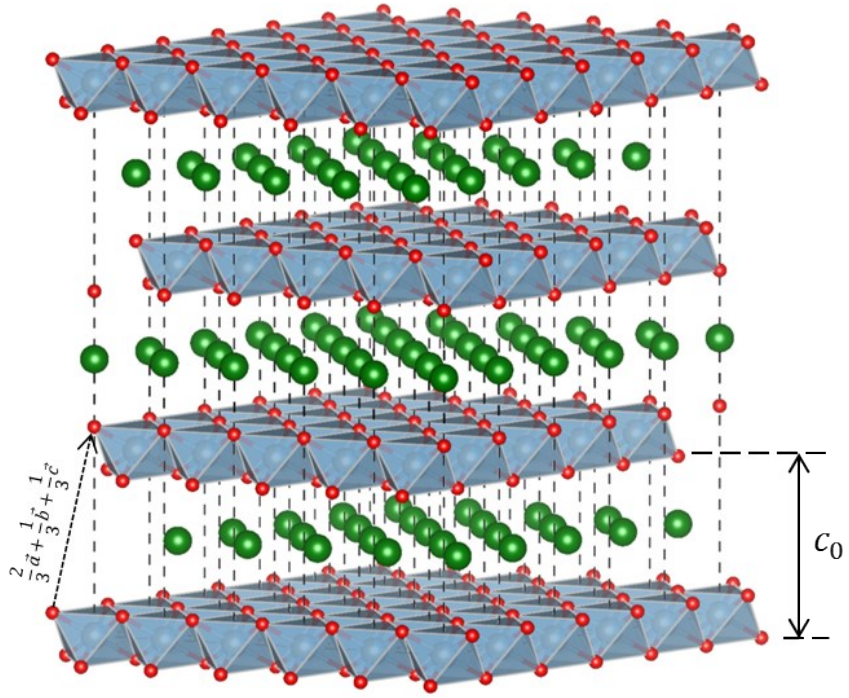

Figure S1. Stacking sequence of layered double hydroxides with polymorphism $3R_1$.

S4. Electron microscopy

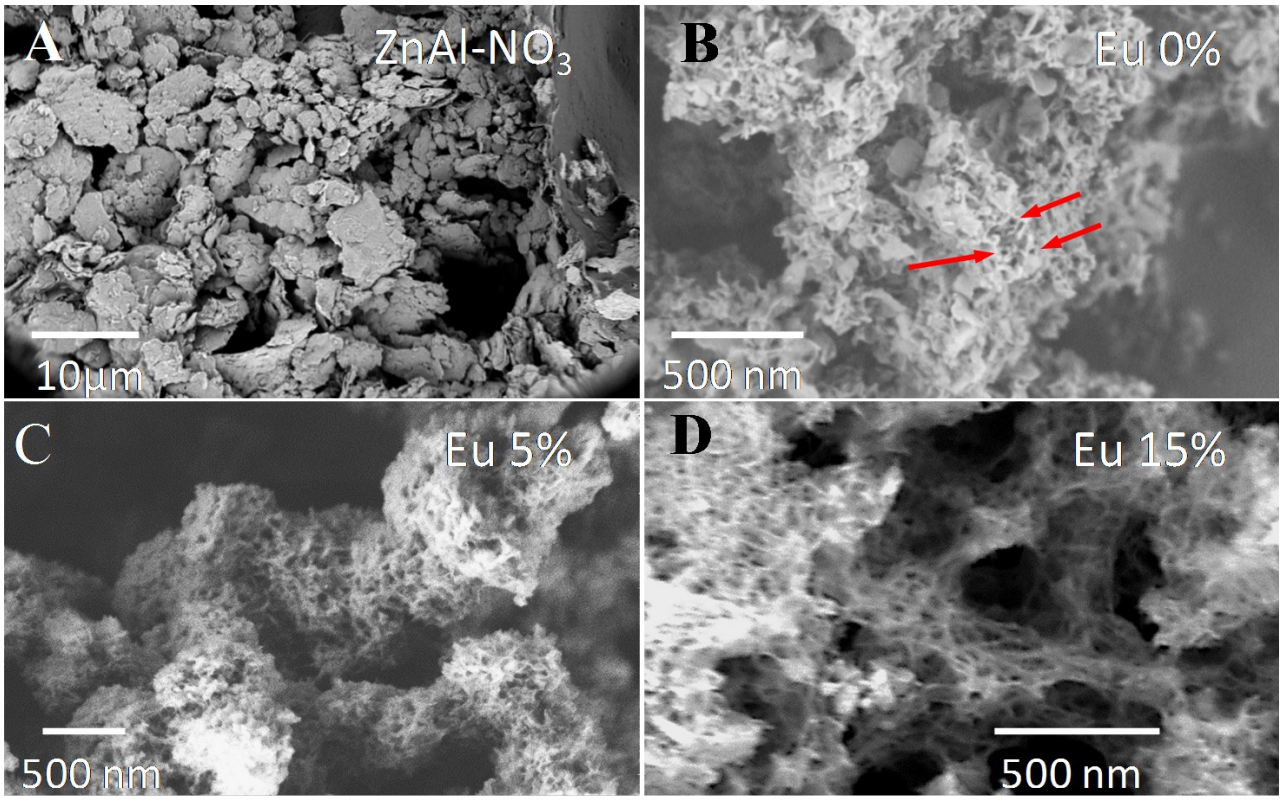

Figure S2. Scanning electron micrographs of (A) ZnAl-NO_3 and (B-D) ZnAlEuX%-BTC-P123 (X = 0, 5 and 15).

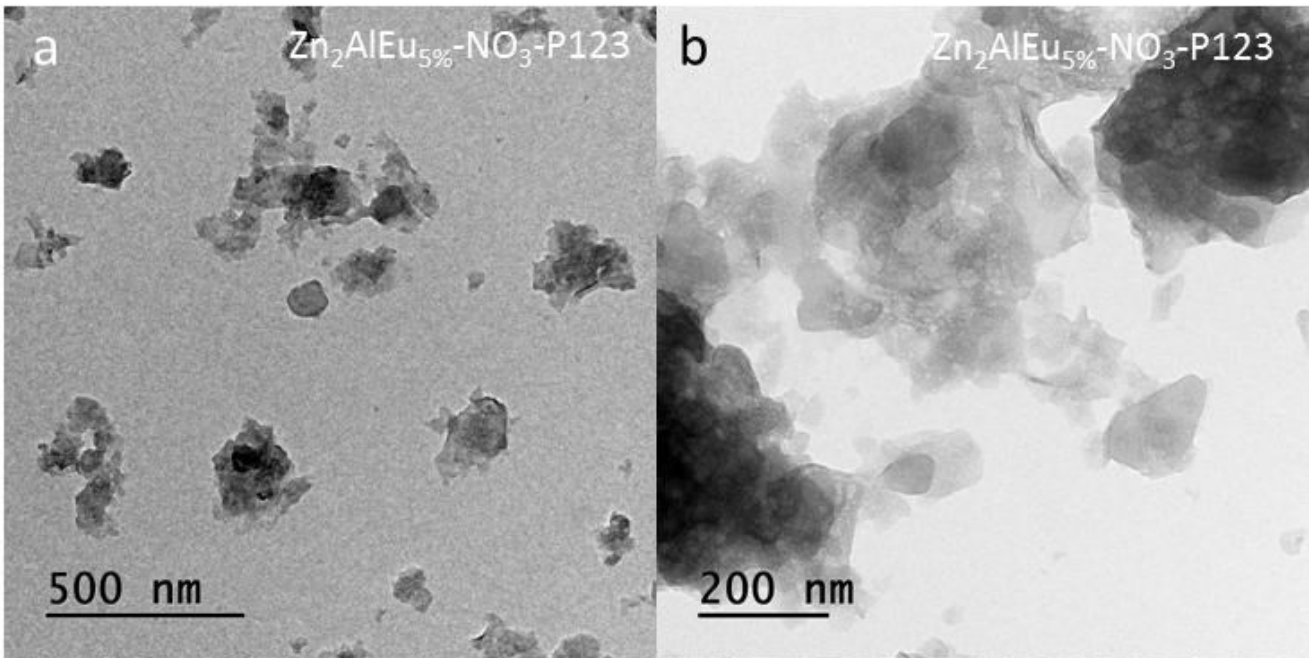

Figure S3. Scanning electron micrographs of the sample ZnAlEu5%-NO_3-P123 showing that the nanotubular morphology is destroyed if BTC is not present in the samples.

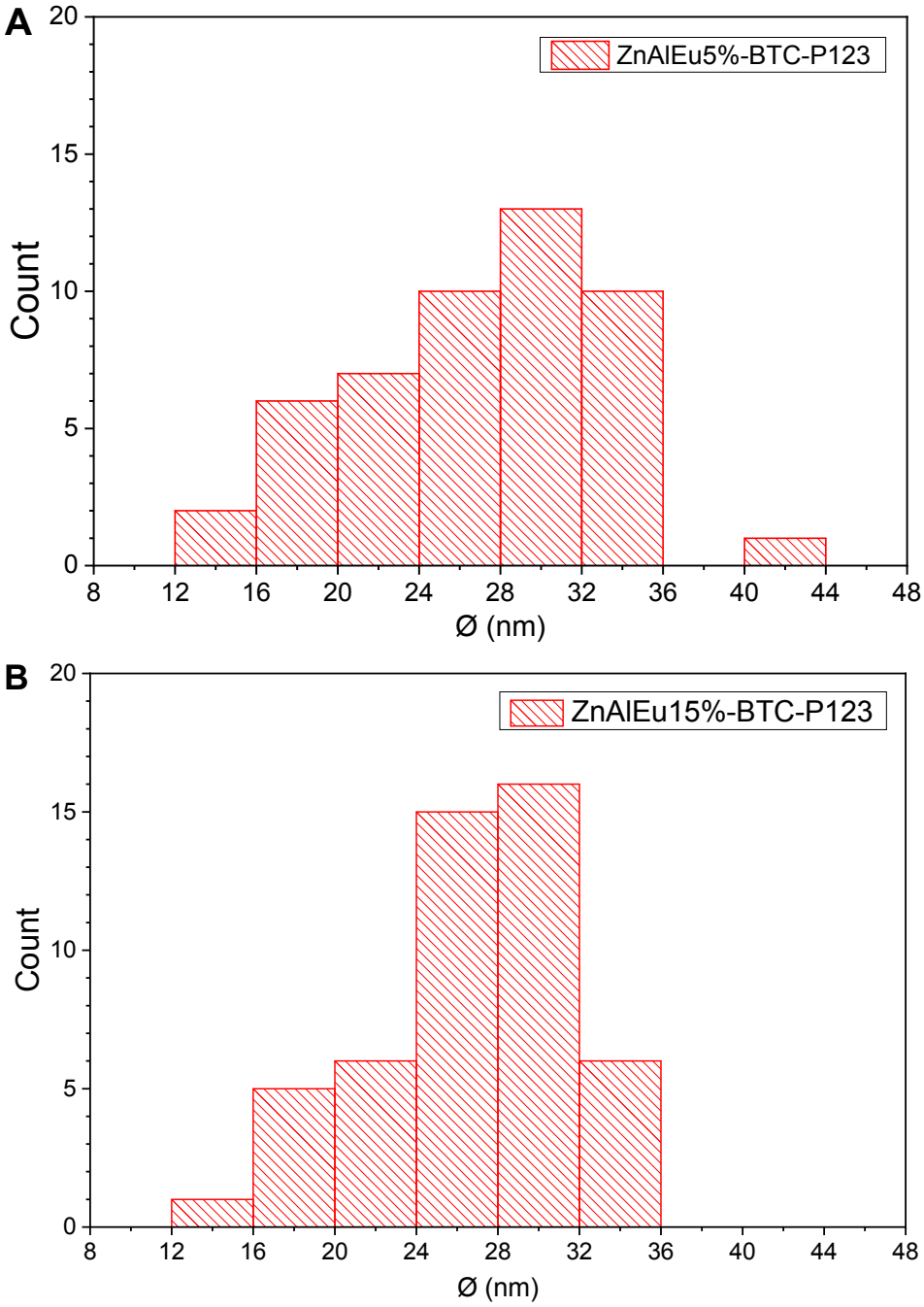

Figure S4. Histogram for the distribution of external diameter of the nanotubes in the samples (A) ZnAlEu5%-BTC-P123 and (B) ZnAlEu15%-BTC-P123. Analysis done on TEM micrographs using the software ImageJ.

S5. Energy dispersive X-ray spectroscopy

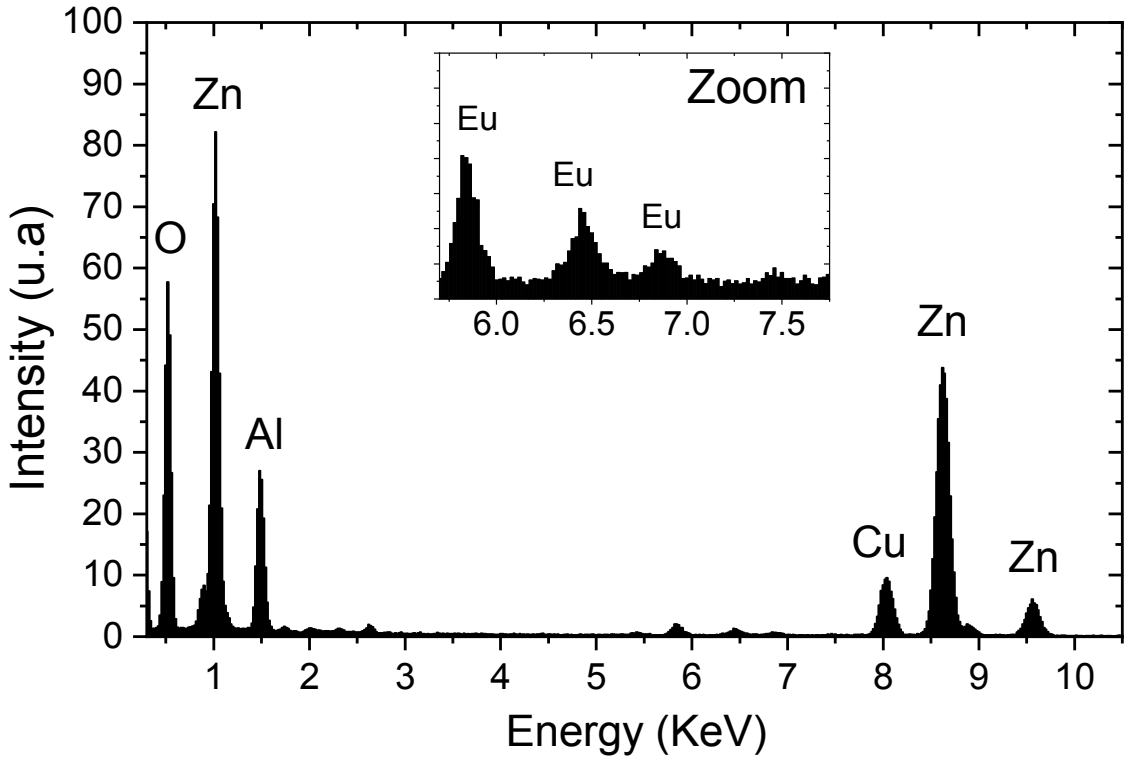

Figure S5. EDX spectrum of the region shown on Figure 2 F. The Cu peak arises from the Copper TEM grid.

S6. X-ray Absorption Near Edge Spectroscopy (EXAFS)

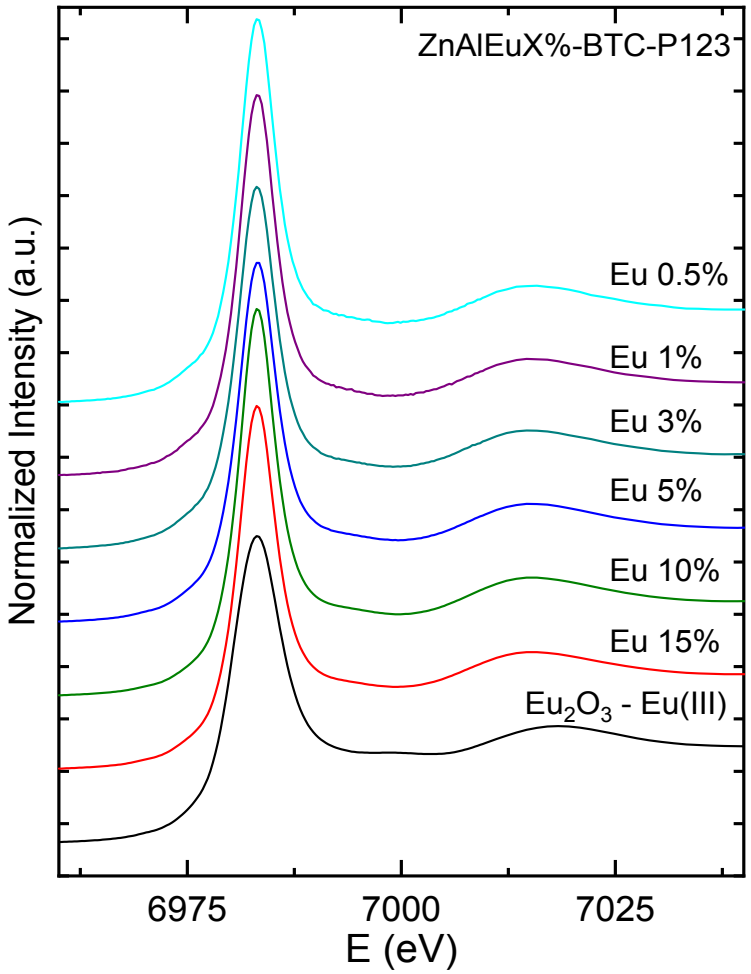

Figure S6. Normalized Eu L^{III}-edge near edge spectra (XANES) for the samples ZnAlEuX%-BTC-P123 (X = 0.5, 1, 3, 5, 10 and 15) (color lines) and the reference compound Eu_2O_3, in which Europium is in the Eu(III) oxidation state.

S7. Extended X-ray Absorption Fine Structure (EXAFS)

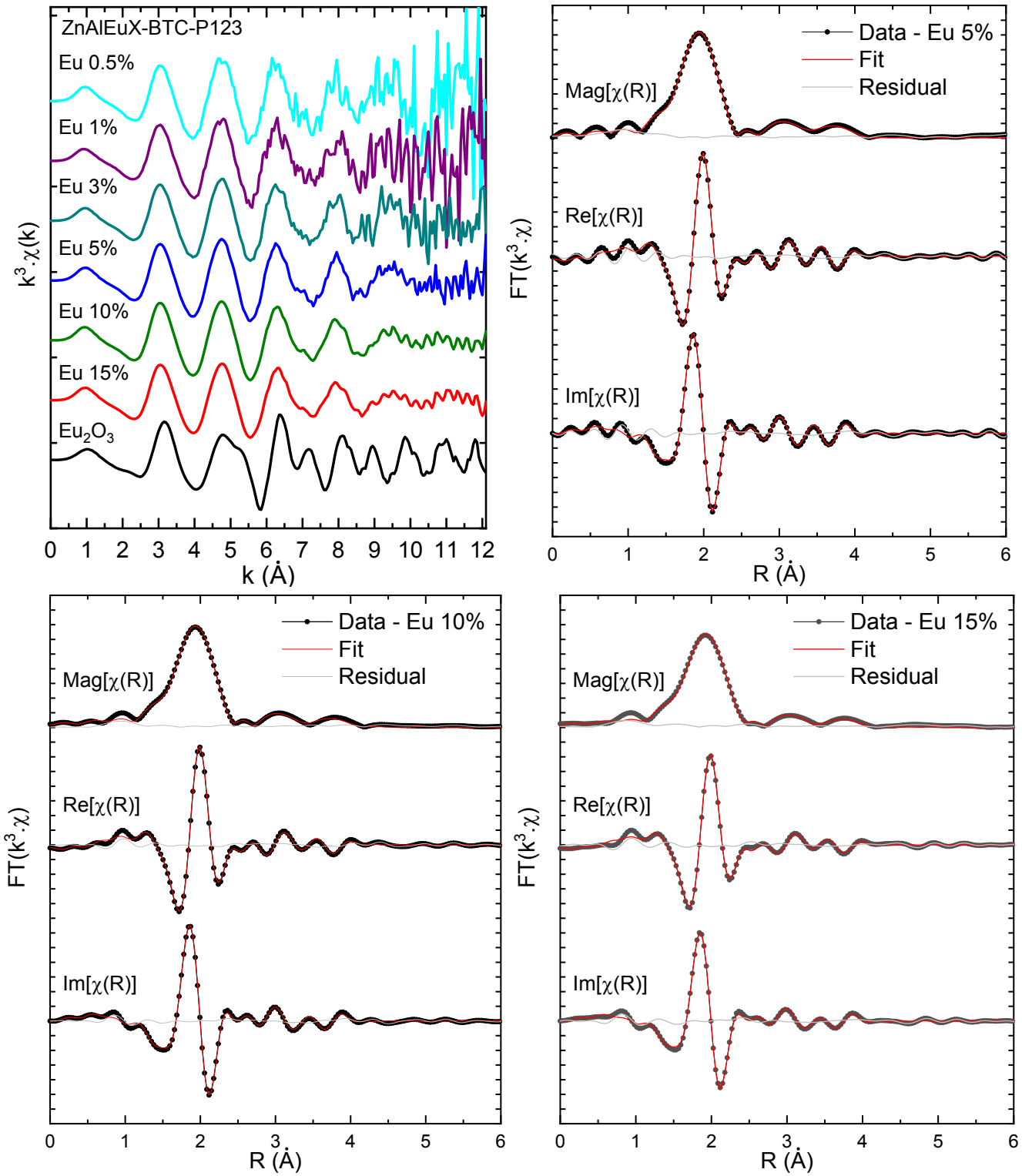

Figure S7. (A) Eu L^{III}-edge XANES spectra for the samples ZnAlEuX%-BTC-P123 (X = 0.5, 1, 3, 5, 10 and 15) and the reference compound Eu_2O_3. Eu LIII-edge Fourier transformed EXAFS spectra of (B) ZnAlEu5%-BTC-P123, (C) ZnAlEu10%-BTC-P123 and (D) ZnAlEu15%-BTC-P123.

Table S5. Comparison between the different models fitted to the Eu LIII-edge EXAFS data for the sample ZnAlEu15%-BTC-P123. These models consider different scatterers for the second and third coordination shells. The first shell comprises Oxygen scatterers. Although all these models produced low R-factors, some parameters have been evaluated to unphysical values.*

	Model 1 (O + O)			Model 2 (Zn + Zn)			Model 3 (Zn + O)		
Path (R_0)	N^A	R (Å)^B	σ^2 (Å^2)^C	N^A	R (Å)^B	σ^2 (Å^2)^C	N^A	R (Å)^B	σ^2 (Å^2)^C
Eu-O (2.4 Å)	7.8	2.419	0.01176	7.1	2.415	0.01105	7.9	2.416	0.01199
Eu-O (3.5 Å)	3.4	3.557	0.01117	-	-	-	-	-	-
Eu-Zn (3.5 Å)	-	-	-	16.5	3.100	0.04823	9.7	3.588	0.02897
Eu-O (4.0 Å)	-2.9	4.186	0.01000	-	-	-	-	-	-
Eu-Zn (4.0 Å)	-	-	-	5.9	4.022	0.02538	-17.5	4.086	0.04236
ΔE (eV)	3.6			3.2			3.1		
R-factor (%)	0.33%			0.76%			0.33%		
Chi-reduced	44			100			44		

* The k fitting range is 2.0-11 Å^{-1}. The R fitting range is 1.0-4.2 Å. ^{A} Coordination number. ^{B} Bond distance. ^{C} Debye-Waller factor.

S8. Photoluminescence spectroscopy

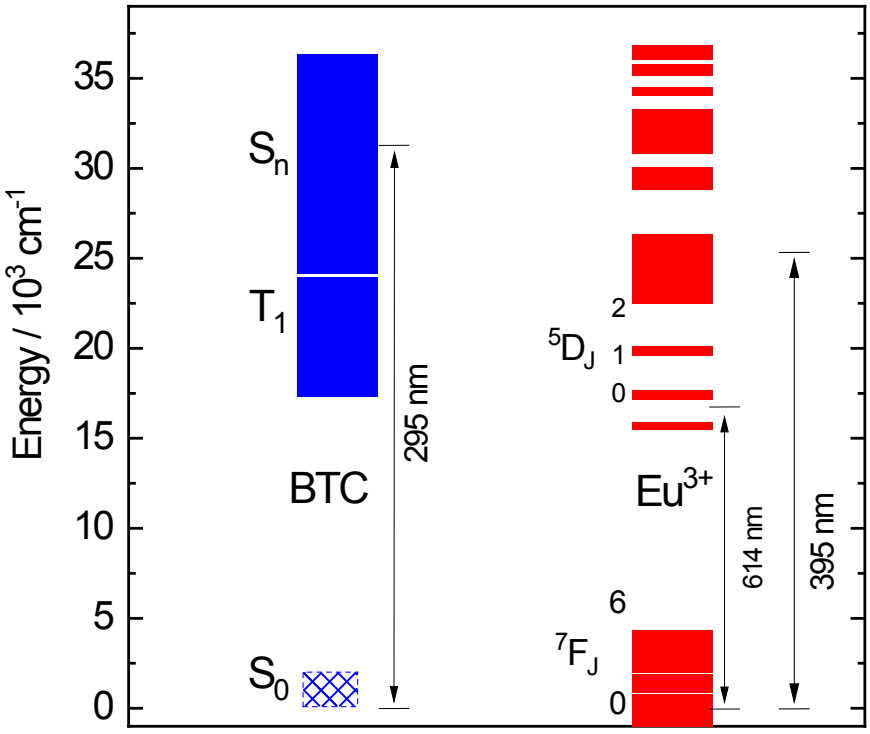

Figure S8. Energy diagram depicting the ligand-to-metal energy transfer from BTC to Eu^{3+}. BTC is excited from the singlet state S_0 to an excited singlet state S_n, following a nonradiative decay to the triplet T_1. From T1, energy is transferred to the quasi-resonant 4f levels of Eu^{3+}. The bandwidth of the S_0 level is unknown and is shown as hatch. Energy levels of BTC and Eu^{3+} according to Refs. [8] and [9], respectively.

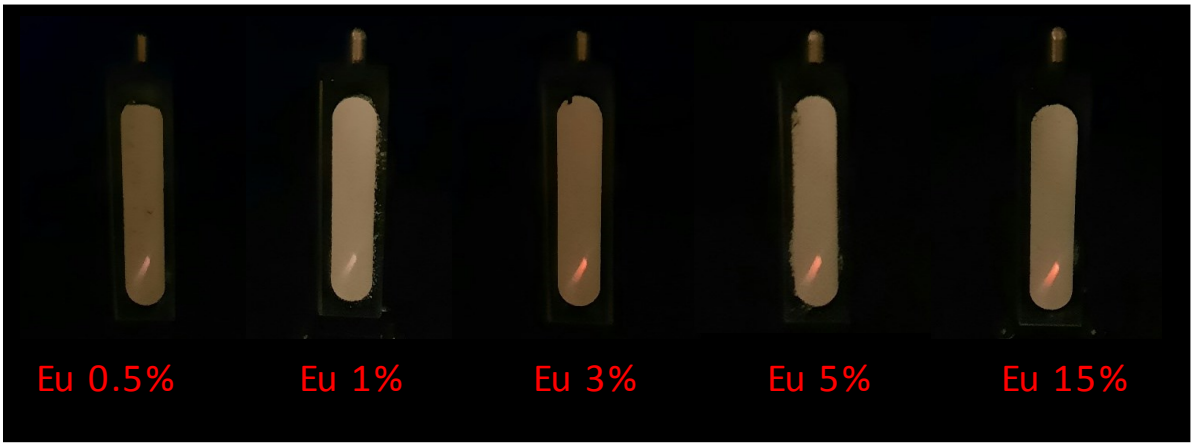

Figure S9. Picture showing the PL of ZnAlEuX-BTC-P123 (X = 0.5, 1, 3, 5 and 15%) under excitation on the BTC excitation band at 294 nm. A 455 nm low pass optical filter has been placed before the less to remove the reflected excitation beam.

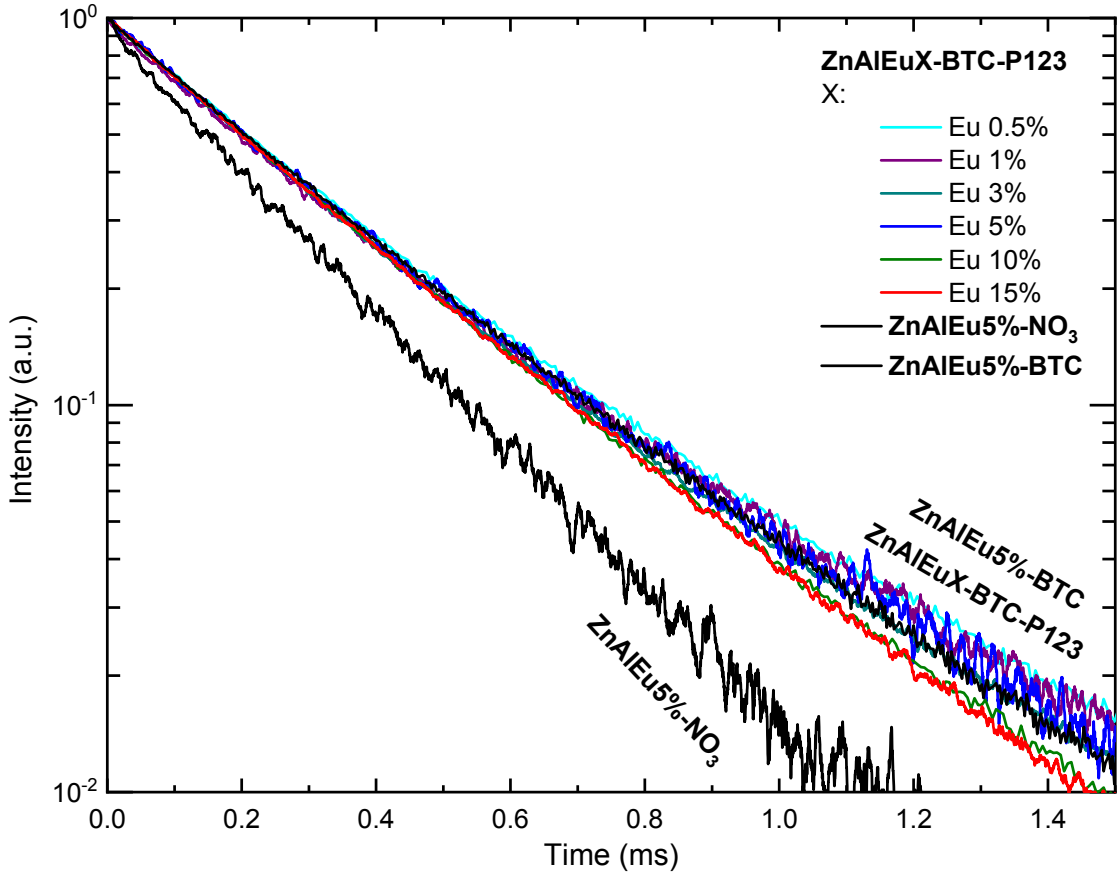

Figure S10. Luminescence decay curves monitored on the $(Eu^{3+})^5D_0 \rightarrow {}^7F_2$ emission band after excitation in the ligand band (295 nm) for samples containing BTC and direct excitation of the Eu^{3+} activators (394 nm) in the nitrate intercalated sample.

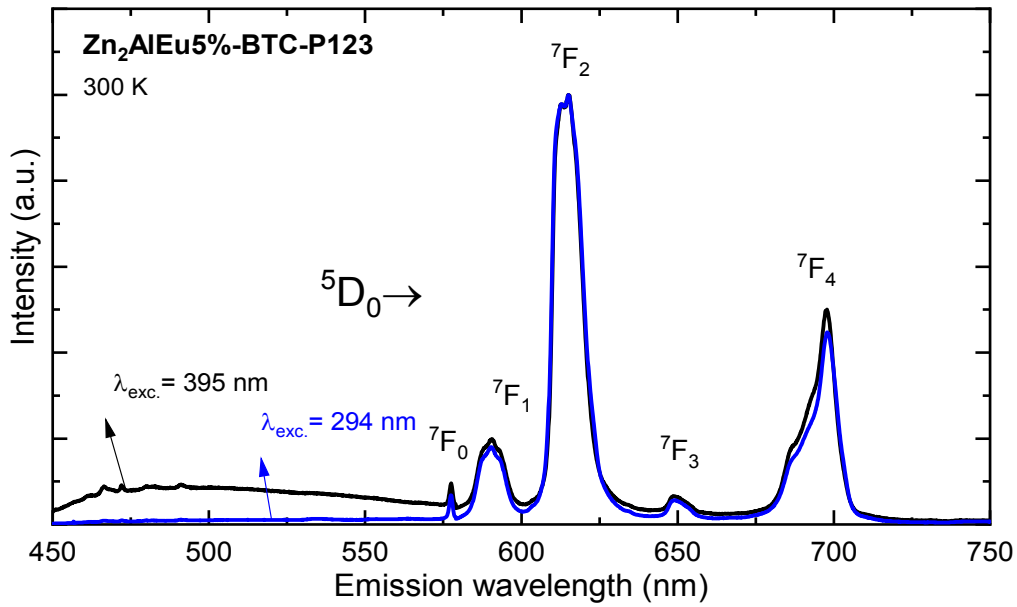

Figure S11. Emission spectra for the sample ZnAlEu5%-BTC-P123 after excitation in the ligand band at 294 nm and direct excitation of the $(Eu^{3+})^7F_0 \rightarrow {}^5L_6$ excitation band at 395 nm. The spectra are normalized by the maximum of the $(Eu^{3+})^5D_0 \rightarrow {}^7F_2$ emission.

S9. Thermogravimetric curves

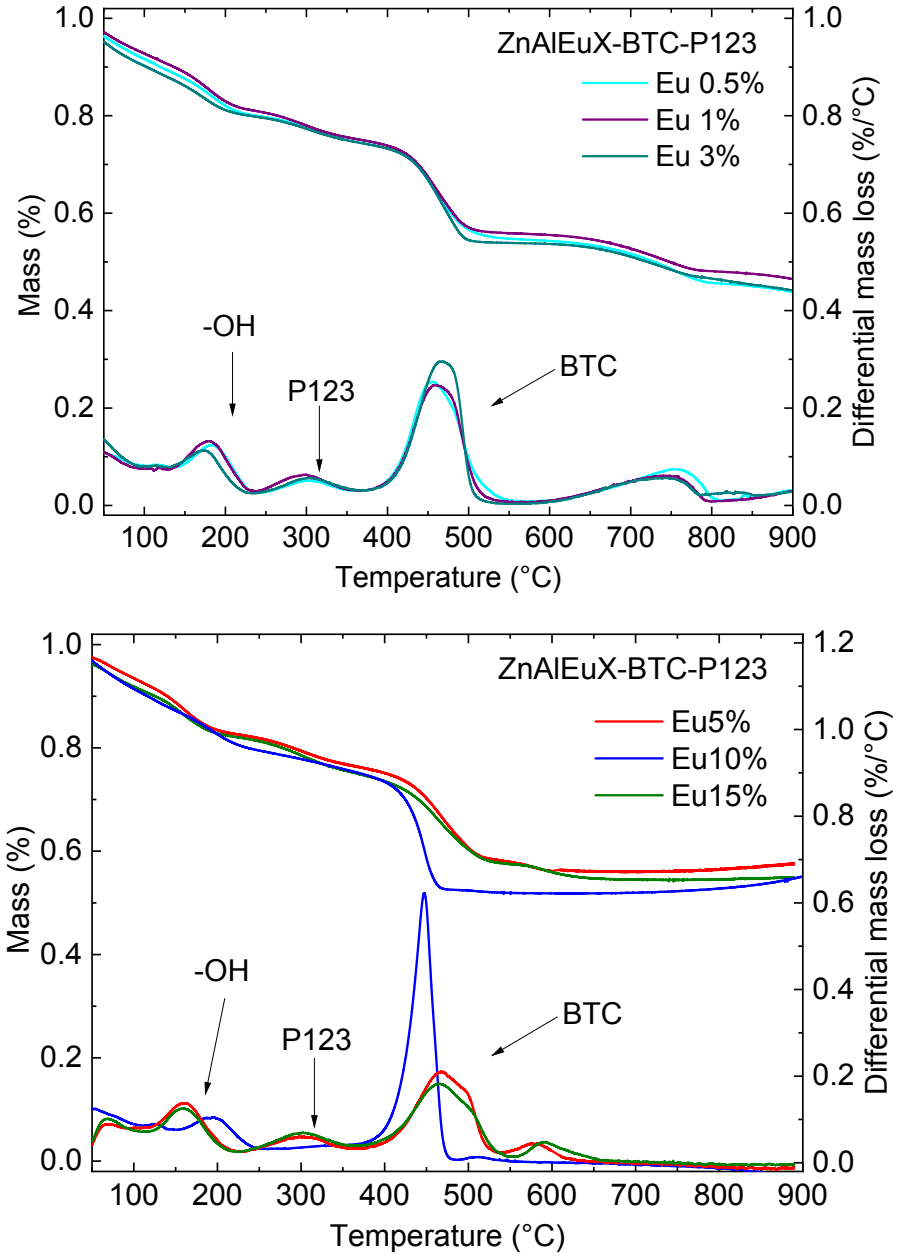

Figure S12. Thermogravimetric analyses used for the determination of the BTC content in the samples with P-123.

References

1 S. J. A. Figueroa, J. C. Mauricio, J. Murari, D. B. Beniz, J. R. Piton, H. H. Slepicka, M. F. De Sousa, A. M. Espíndola and A. P. S. Levinsky, *J. Phys. Conf. Ser.*, 2016, **712**, 12022.

2 Z. K. Heiba, Y. Akin, W. Sigmund and Y. S. Hascicek, *J. Appl. Crystallogr.*, 2003, **36**, 1411–1416.

3 A. F. Morais, I. G. N. Silva, B. C. Lima, F. A. Garcia and D. Mustafa, *ACS Omega*, 2020, **5**, 23778–23785.

4 I. G. N. Silva, A. F. Morais, B. C. Lima, F. A. Garcia and D. Mustafa, *Appl. Clay Sci.*, 2020, **199**, 105861.

5 J. J. Rehr and R. C. Albers, *Rev. Mod. Phys.*, 2000, **72**, 621–654.

6 B. Ravel and M. Newville, *J. Synchrotron Radiat.*, 2005, **12**, 537–541.

7 F. Geng, H. Xin, Y. Matsushita, R. Ma, M. Tanaka, F. Izumi, N. Iyi and T. Sasaki, *Chem. - A Eur. J.*, 2008, **14**, 9255–9260.

8 E. R. Souza, I. G. N. Silva, E. E. S. Teotonio, M. C. F. C. Felinto and H. F. Brito, *J. Lumin.*, 2010, **130**, 283–291.

9 W. T. Carnall, P. R. Fields and K. Rajnak, *J. Chem. Phys.*, 1968, **49**, 4412–4423.